Experimental contribution to the understanding of wetting of solid surfaces at the meso- and nano-scale using dynamic AFM

A.B. Jódar-Reyes[1], A. Méndez-Vilas[2,*], and M.L. González-Martín[2]

[1]Department of Applied Physics, University of Extremadura, Facultad de Veterinaria, Avda. Universidad s/n, 10071, Cáceres, Spain.
[2]Department of Applied Physics, University of Extremadura, Campus Universitario, Avda. de Elvas s/n, 06071, Badajoz, Spain.

Despite the extensive modelling effort pursuing an understanding of the wetting behaviour of microscopic and sub-microscopic liquid droplets on solid surfaces, experimental results on this issue are still rather scarce. Atomic force microscopy (AFM), operated in dynamic modes (non-contact or intermittent contact) is expected to become a formidable tool to investigate wetting at those scales. It ensures extremely high spatial nanometer-lateral and sub-Ångström-vertical resolution, while the most recent advances are rapidly improving its temporal resolution, which will benefit the study on dynamical processes. However, the study on how liquid micro and nano-droplets behave on a particular surface is still far from being routine, and many authors recognize that setting the optical parameters for getting stable images of liquid interfaces has a still significant trial-and-error component. This is mainly due to the strong mechanical instabilities that may arise in a narrow space over the surface during the normal operation of the AFM, and that may depend on a variety of factors such as the cantilever spring constant, amplitude of oscillation, noises introduced in the optical detection system which may influence the probe movement, surface tension and evaporative behaviour of the probed liquid or wetting of the AFM tip by the probed liquid. In spite of these current drawbacks, an intensive effort is being currently made for controlling and understanding the effect of such parameters on the acquisition of AFM images of liquid interfaces. The main experimental results are reviewed in this work, with a focus on the comparison with traditional macroscopic wetting studies and the potential practical applications of having reliable AFM images of liquid micro and nano-droplets deposited onto solid substrates.

Keywords: AFM; Atomic Force Microscopy; wetting; nanoscale; nano-wetting; non-contact; intermittent-contact; tapping; nano-droplet; surface tension.

1. Introduction: wetting and contact angle.

To illustrate the wetting phenomenon, let us consider a small amount of liquid in contact with a solid. In one extreme case the liquid can wet the solid so well that it spreads completely. In the other extreme it avoids any contact with the solid and the droplet retains its individuality upon contact. Whether or not wetting occurs depends on the affinity of the liquid for the surface. If the liquid is water and the surface is hydrophobic, no wetting is expected. Conversely, wetting by water will take place on hydrophilic surfaces. Between these extremes there is a range of intermediate situations in which the liquid meets the solid at a certain angle called the contact angle, θ (Figure 1). The better the wetting, the sharper the angle. In fact, the contact angle can be taken as a measure of the relative hydrophilicity or hydrophobicity of the solid [1]. Even further, contact angle studies are used to gain insight into the fundamentals of wetting in many systems (e.g. adhesives, lubricants, and cell adhesion to biological membranes) [2,3].

* Corresponding author: e-mail: amvilas@formatex.org

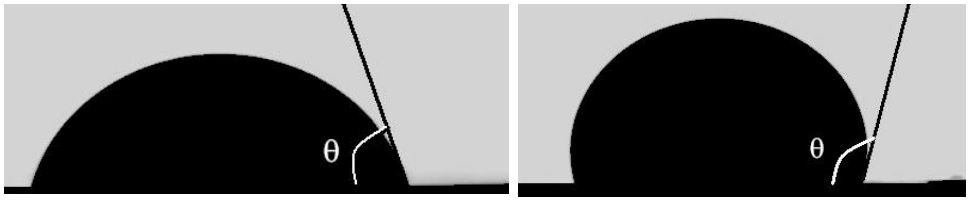

Fig. 1. Solid partly wetted by liquid (left); solid poorly wetted by liquid (right).

2. Why are liquid micro- and nano- droplets important for current wetting research?

2.1. They are necessary for evaluating wetting properties of miniaturized systems.

Using micro- and nano- water droplets can be envisaged as a relatively simple method to test the surface contamination of small parts of a device. For example, as-received AFM tips and cantilevers (which have microscale length and width and nanoscale thickness) are known to be coated by a thin hydrocarbon layer, which if not removed, may affect force measurements, both in air or in a liquid environment. While classical surface-sensitive methods can be applied to evaluate the surface contamination of an AFM cantilever, they are usually quite expensive, time-consuming and require a vacuum. This contamination of the AFM cantilever in the vicinities of the tip apex has been proposed to be responsible for the increase in the adhesion force detected in force spectroscopy studies in water [4]. Bonnacurso *et al.* undertook an elegant experiment [5] in which microscopic water droplets were placed directly onto AFM cantilevers to test the effectiveness of cleaning procedures. Results are presented in Figure 2. Before plasma cleaning, the drop forms a contact angle of $\theta = (60 \pm 4)^{\circ}$; after plasma cleaning, the drop forms a contact angle of $\theta = (14 \pm 6)^{\circ}$. This allowed an in-situ local characterization of the cantilever contamination near the apex through a simple parameter such as the contact angle.

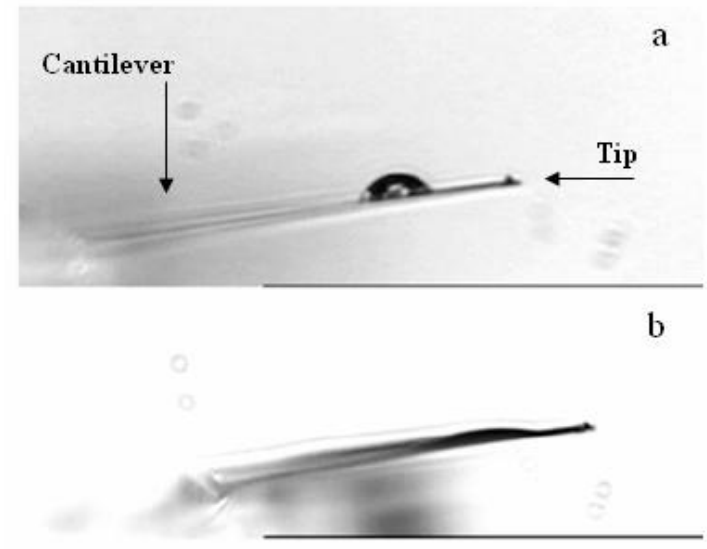

Fig. 2. Sequence of two images showing a water drop deposited on a V-shaped Si_4N_3 cantilever before (a) and after (b) plasma cleaning. Reproduced with permission from [5]. © 2005 American Chemical Society.

This case clearly illustrates how the ability of depositing ultra-small liquid droplets on parts of miniaturized systems (Micro and Nano Electro Mechanical Systems (MEMS/NEMS), for example) could serve as a very useful, relatively simple and rapid way to test the state of a surface.

2.2. They permit assessing the heterogeneity of the surface at micro or nano scale in terms of topography or physico-chemical properties

While macroscopic contact angle measurements provide an averaged information on the wettability of the material substrate by the probing liquid over a large area, the use of micron or sub-micron sized droplets allows one to quantify wetting properties at a much more local level, provided that the number of molecules included in the droplets is high enough to for the correct application of thermodynamic concepts. This spatially resolved wetting measurement permits the evaluation of the homogeneity of the physico-chemical parameters of an extended surface, at a quite high resolution. For instance, Connell *et al.* [6] used intermittent-contact AFM and obtained small contact angle values of oil nano-droplets on polystyrene (PS), but constant over a large number of droplets (13 ±2)º, which indicated the homogeneity of the PS surface at the nanoscale. In general, it is expected that the characterization of wetting properties of surfaces at the nanometer scale will be important in getting a more local view of different important phenomena in chemistry, electrochemistry, biology, and technology, such as the adsorption behavior of proteins and surfactants [7,8], or the atmospheric corrosion mechanism [9,10]. In particular, they will allow one to asses how homogenous a surface is, at a quite local level, and in a relatively direct and easy way. This is indeed important as chemical heterogeneity is known to be one of the factors which influences contact angle measurements, jointly with surface roughness, which in contrast can be accurately described in a wide range of scales using atomic force microscopy [11,12].

2.3. They constitute the ideal systems for direct experimental determination of the contact line tension (CLT).

The contact line tension (CLT), defined as the excess free energy of a solid-liquid-vapor system per unit length of the contact line, or equivalently the linear tension due to the imbalance of intermolecular forces experienced by molecules located in and around the three phase confluence zone, can affect the observed contact angle [13], especially when reducing the size of the system and surface forces play a major role [14]. It is analyzed through the "modified Young equation":

$$\cos(\theta) = \cos(\theta_{\text{Young}}) - \frac{1}{\gamma_{\text{LV}}}\tau\kappa \qquad \text{eq. 1}$$

where κ is the local curvature of the contact line where the local contact angle gives θ, γ_{LV} is the surface tension of the liquid, and τ is the line tension. The contact angle θ_{Young} is the one that obeys the Young equation:

$$\cos(\theta_{Young}) = \frac{\gamma_{SV} - \gamma_{SL}}{\gamma_{LV}} \qquad \text{eq. 2}$$

Where $\gamma_{SL,}$ and γ_{SV} are the interfacial tensions between solid/liquid, and solid/vapor, respectively.

Both the local curvature and contact angle can be obtained directly from an AFM image of the liquid droplet resting on the solid substrate. The former, by fitting a specific portion of the contact line to a circle, and the latter, from a height profile taken across a line perpendicular to the portion of the contact line where the local curvature has been computed. The magnitude of this tension is very small

(theoretical estimations are around 10^{-11} N), and it becomes dominant only at the nanoscale. In fact, a characteristic length scale for the influence of this tension can be estimated by dividing a typical CLT value to a typical surface tension value, i.e., 10^{-11} J/m / 10^{-2} J/m^2 = 1 nm. [15]. If the line tension is extremely small (10^{-12} N or less) it would be operative in systems with molecular dimensions only, and its practical importance would be limited. On the other hand, if line tension values are orders of magnitude larger than 10^{-12} N, then it may become a factor in analyzing or designing systems of technological application. For instance, in microfluidic circuits, patterned surfaces are used to control wettability; in such cases, limits arise from small lateral scales involving high local curvature for three-phase line. Consequently, the line tension will contribute to the fidelity of such patterned surfaces to control wettability. In froth flotation, the modification of the contact angle by the line tension may promote or hinder particle wetting and displacement into the aqueous phase. It has been found that particles of irregular shape, especially with sharp edges, will resist the immersion into the liquid phase because of line tension effects [16]. The small magnitude of the line tension requires considerable ingenuity in experimental design. In the existing techniques, line tension is indirectly found by measuring parameters such as contact angle or particle size and using theoretical expressions. The majority of experimental studies for solid-liquid-vapor systems reviewed elsewhere [14] reported a positive sign for the line tension, ranging from 10^{-9} to 10^{-6} N, but they used drops of macroscopic size. A general consensus has not been reached yet, even on the physical origin of the line tension, and the issue of the contribution of a line tension to the variation of the contact angle with drop size is still a controversial issue in wetting research. In any case, the demonstrated capability of atomic force microscopy to give detailed topographic profiles at a spatial resolution well below the traditional optical techniques, and its ability to get such profiles on liquid structures of dimensions where the line tension is expected to have a notable influence, might definitively contribute to clarify such a fundamental issue, and provides an accurate imaging tool for more applied wetting measurements.

2.4. They make possible the quantification of the liquid surface tension at the nanoscale. In general, they permit the evaluation of the surface tension dependency on the droplet size in the micron and sub-micron range.

Once stable micron or sub-micron sized droplet images have been taken, force spectroscopy allows one to quantify the interaction forces between the AFM tip and the fluid surface directly. Here, the critical point is to know the mechanical properties of the AFM cantilever, and specifically its spring constant, which is known to largely differ from the manufacturers' specifications [17]. Several techniques exist for measuring the cantilever spring constant, which permit to know its value with an uncertainty of at least 20% [18].

By assuming that the air-liquid interface and the AFM tip act as two linear springs in series, over a small deflection, the system spring constant or the interfacial tension can be expressed as

$$K_{interf} = \frac{K_{cant}}{\frac{d_{hard}}{d_{interf}} - 1} \qquad \text{eq. 3}$$

where K_{interf} is the effective spring constant of the interface, K_{cant} the measured spring constant of the cantilever, d_{hard} the cantilever deflection per unit piezo translation when pushed against a hard surface and d_{interf} the cantilever deflection per unit piezo translation when pushed against the air-liquid interface. The situation is drawn schematically in Figure 3.

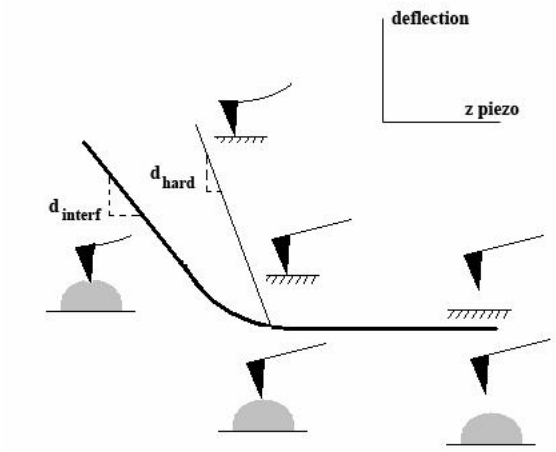

Fig. 3. Schematic drawing showing the AFM cantilever deflection as it approaches, touches and pushes a hard and a liquid surface. The extension of the contact part has been exaggerated; in a real experiment it should be kept as small as possible so that the interaction between the liquid surface and the AFM tip can be modeled as two linear springs in series, and also to avoid capillary wetting of the tip.

Connell *et al.* [6] applied this approach for the determination of the interfacial tension of hydrocarbon nano-droplets of 20-400 nm in diameter resting on a PS substrate (Figure 4). A reasonable good approximation to the known interfacial tension was obtained. A similar approach based on the interaction force between a sharp AFM tip and a fluid interface was used by Fraxedas *et al.* [19] for determining the surface tension of water using confined nano-droplets of about 150 nm in diameter. In this case, quite a large surface tension was obtained with respect to the well known macroscopic value (0.073 N/m), although it is to be noted that confined nano-droplets were used in this case. Clearly, this capability of an AFM of deforming fluid interfaces with controlled loads while recording the mechanical response of the cantilever has full potential for elucidating the structure and interfacial properties of liquid nanostructures or liquids in confined geometries. This is the situation in microfluidics [20], especially in droplet-based microfluidics applications [21,22], and in a large amount of biological structures such as pores and channels.

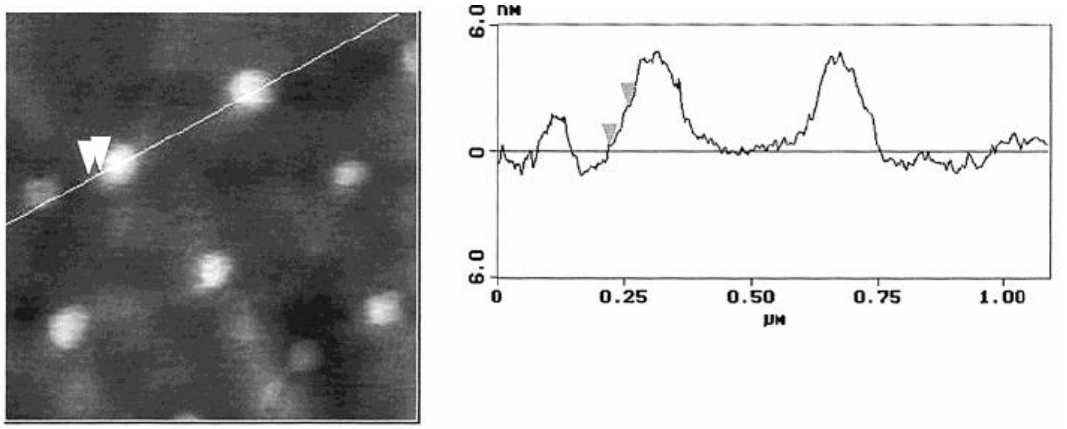

Fig. 4: Cross-sectional profile of oil droplets on a PS surface in water, taken in intermittent-contact AFM. Height of the droplets was about 5 nm and contact angle 4-5º. Reproduced with permission from [6]. ©2002 American Chemical Society.

3. Experimental quantitative wetting studies using dynamic AFM.

AFM is the best suited instrument for imaging nanometer-scale liquid droplets on flat surfaces because of its nanometer-scale resolution and its capability of operating in air or under controlled atmospheres on any macroscopically flat substrate [19]. Although mainly used for surface characterization of solid surfaces, AFM has also demonstrated its suitability for imaging the surface of liquid structures in different operation modes. The formation of stable mesoscopic and nanoscopic droplets on solid surfaces in order to determine contact angles is not trivial. Different methods can be found in the literature and results are reviewed in this section.

3.1. Non-contact AFM (NC-AFM).

Different authors have observed liquid micro- and nano-droplets and other liquid structures on different materials by NC-AFM. In this imaging mode, the AFM tip is brought close to the surface while vibrating at a frequency slightly higher that the intrinsic resonance frequency of the cantilever, and at certain amplitude (very small, ideally below 10 nm). It is approached to the surface until the amplitude has decreased to a pre-set value (set-point amplitude) due to the long-range attractive forces. This set-point amplitude is kept constant through the whole scanning by the feedback system. The sensing is based on long-range weak forces, so the probe doest not make physical contact with the surface. The disadvantage is that as it is based on long range forces, it suffers from a reduced spatial resolution. Also the fluid adsorbed layer which is present at every surface exposed to air may interfere, and capillaries might form between it and the probe, producing instabilities due to jump-to-contact. This makes true NC-AFM rather difficult to achieve in air.

Gil *et al.* [23] imaged molecularly thin water films on hydrophilic mica, gold, and highly oriented pyrolitic graphite (HOPG). On mica, they found islands of water layers of 0.7 and 1.4 nm in height working at relative humidities (RH) of (2-95)%. On graphite, they found rounded and flat water islands of about 5 nm in height (at RH 90%). These islands tend to move around, coalesce, and form larger islands. The tip is thought to be responsible for the condensation of water on the surface. With time, these islands evolve and show in addition to the 5nm high layer a second lower one. When the surface is left overnight at 90 % RH, the higher terrace completely disappears and only islands of about 2 nm remain. Their perimeter is oriented preferentially along the high symmetry direction of the graphite crystal which is thought to be related to a solid-like character of the layer. Under this assumption the 2 nm thick layer could be formed by 6 bilayers of crystalline water. Both 5 and 2 nm islands completely disappeared from the surface after some hours when the RH decreased to very low values (2 %). On gold surfaces, they found water layers of 2 Å in height. This corresponds to the diameter of a single water molecule.

Wang and coworkers [9,10] imaged micro water droplets on mica and different metal surfaces. On mica, they observed water droplets with average height of 7.1 nm and average radius of 78 nm. The corresponding contact angle was 10.8º. They also used this imaging mode to observe water droplets on polished, air oxidized and pure water immersed pure chromium, nickel, iron and SUS304 steel surfaces. The main characteristics of the micro droplets on each surface and the corresponding average contact angle obtained by assuming a spherical cap overall form of the droplet profile are included in table 1, which will be discussed later. The corresponding macro-contact angle is also presented. The morphologies of oxidized and water immersed pure iron could not be observed because its surface was not flat.

Checco *et al.* [24] measured the contact angle of microsized and nanosized alkane droplets partially wetting a model substrate (silanized silicon wafers) using NC-AFM. Minimal heterogeneity and pure van der Waals interactions were ensured. Because of the volatility of alkanes, stable droplets could not be formed under ambient conditions. Then, they designed an evaporation-condensation chamber connected to the AFM scanning head. The large range of droplet sizes accessible using this technique allowed them to determine the contact line curvature dependence of the contact angle with unprecedented accuracy.

The droplet profiles were fitted to a spherical cap providing an accurate determination of the contact angle and contact line tension. The contact angle decreased with decreasing drop radius from the macroscopic values. An important result is that the modified Young equation does not correctly describe the experimental data when a large enough range of droplet sizes is considered. Whereas previous studies explain such a dependence by a line tension effect, their results and calculations on a model system point to an extreme sensitivity to weak substrate heterogeneities confirmed by numerical simulations. In a more recent paper, these authors [25] measured the contact angle of ethanol stripes formed in an evaporation-condensation chamber on a patterned surface consisting of hydrophobic COOH terminated lines and methyl groups terminated hydrophilic lines. Ethanol totally wetted the hydrophobic lines, while it did not wet the hydrophilic ones. The apparent contact angle at the stripe's boundary was 12 ± 1º, a value significantly lower than the contact angle measured with a micrometer-sized ethanol droplet on a uniform octadecyltrichlorosilane (OTS) surface (30 ± 1 º). NC-AFM has been also applied to the study of the local wetting of human hair, another attractive micro-system for current beauty care science [26]. Two different techniques are used depending on the nature of the liquid. For nonvolatile liquids, small drops of liquid were directly deposited on the solid by using a microsyringe. For volatile liquids, a condensation technique was used.

3.2. Intermittent-contact AFM (IC-AFM)

IC-AFM (or Tapping mode^{TM}) has been also used to study micro and nano wettability of solid surfaces. This mode avoids that strong contact forces can affect imaged water droplets (contact mode), and the unstable feedback due to the small signal (non-contact mode). It is based on relatively strong short-range repulsive forces between the probe and the surface, which are in a physical contact only during a very short fraction of the oscillation period. Oscillation amplitudes are higher than in the case of NC-AFM.

Pompe *et al.* [27] determined the contact line tension of a three-phase solid-liquid-vapor system from the liquid surface topography data obtained with scanning force microscopy using IC-AFM. The data were analyzed in two complementary ways, one based on the modified Young equation (eq. 1), and the other on the effective interface potential derived from the profile of the liquid-vapor interface in the three-phase region. The two methods agree quite well for the systems investigated. In order to create liquid surface topographies with high contact line curvatures, substrates with an artificial striped wettability pattern were prepared. Hydrophilic and hydrophobic domains with a periodicity between 200 and 1000 nm were obtained. When a micron sized liquid droplet is deposited from the aerosol phase onto the patterned surface, the liquid arranges into its equilibrium shape. Effects of contact angle hysteresis were not observed. From sections through the topographic images taken perpendicular to the contact line at the point of interest, it is possible to determine the local contact angle as well as the local contact line curvature along the contact line. These authors found contact line tensions in the range of 10^{-11} to 10^{-10} J/m. They are lower than the ones reported by other authors [14]. Whereas Pompe *et al.* attributed it to the limited resolution of the microscopy techniques used (optical microscopy), other authors have attributed it to the fact that the characteristics of the surface are far from the ones required for the model used [14].

Mugele *et al.* [28] used IC-AFM to image hexaethylene glycol (HEG) droplets on silanized silicon substrates. Radii between 380 and 8000 nm (which evaporated in several hours) were achieved using an aerosol in a closed container using a standard vaporizer. The droplets were allowed to settle down on a substrate by gravity and AFM imaging was performed under ambient conditions. They averaged the contact angles obtained at each point of the contact line. This is achieved by extracting profiles locally perpendicular to the contact line at each point of the latter. The local contact angles are obtained from the slopes of parabolic fits to these profiles at their intersection with the substrate. For the fits, they excluded the region within 10 nm above the substrate to avoid any possible influence of interfacial force or other possible disturbances. The same contact angle was obtained for all the droplets imaged in the mentioned

range of dimensions, which was also very similar to the macroscopoic one measured optically using milimeter-sized droplets (24º).

Fraxedas *et al.* [19] predicted the surface tension of water nano-droplets in molecular nano-beakers by using this imaging mode.

In a more applied report, Karis and Yayak [29] used IC-AFM to reveal a new type of contamination of magnetic recording slider disks. As the size and flying height of these systems evolve to smaller dimensions, previously insignificant levels of contamination begin to play a role in slider media tribology. This mode was used to characterize nanodroplets formed when hygroscopic ultrafine airborne particles (cloud condensation nuclei) deposit on electrostatically charged thin film magnetic recording disks from ambient conditions. These liquid-like and viscous nanodroplets were found to be responsible for the anomalous results in earlier low-flying height sensitive friction and acoustic emission experiences. [30].

Spagnoli *et al.* [31] imaged and characterized the height and contact angle of ordered water layers formed by wetting/dewetting processes on mica at different states of hydration by tapping mode. The structured layer of 3.3 Å in height closest to the mica surface was based on an icelike layer of hexagonally arranged water molecules.

The authors have recently analyzed the hydrophobicity of silicon wafers at a mesoscopic level [32]. For doing this, contact angles of water droplets with diameters in the range (430±100) nm formed on a silicon wafer sheet were determined from IC-AFM images. Nano-droplets with regular profile were formed by using a sprayer and by working at a high humidity environment (>80%). In order to explore the surface of the naturally oxidized silicon wafer at the nanoscale, before using it for the measurement of nano-droplet contact angles, the dewetting process was monitorized under ambient conditions using an atomic force microscope. Once the retreat of the macroscopic water was evident from the coupled optical microscope, AFM showed the persistence of droplets-films of micrometric lateral dimensions and nanometric vertical dimensions [33], in a first stage of dewetting. In Figure 5a an example of these structures are presented. Both a topography (left) and an amplitude (right) image, which is useful for a better visualization of the edges of the present structures, are shown. These rests naturally evaporated in about an hour. Only a few examples can be found in the literature monitoring the dewetting behavior of a volatile liquid on a solid surface, mainly due to the difficulties in getting stable images rapidly after the droplets deposition. It is remarkable the high similarity of this water dewetting pattern with those published by Haferl *et al.* [34] (Figure 5b) while monitoring the dewetting of 1,5-pentadeniol under ambient conditions, even at such different dimensional scales. This extraordinary similarity of the dewetting pattern suggests that the same physical mechanism is governing the de-wetting at both scales. In particular, this suggests that the sub-microscopic water structure seen in Fig. 5a fully behaves as a liquid.

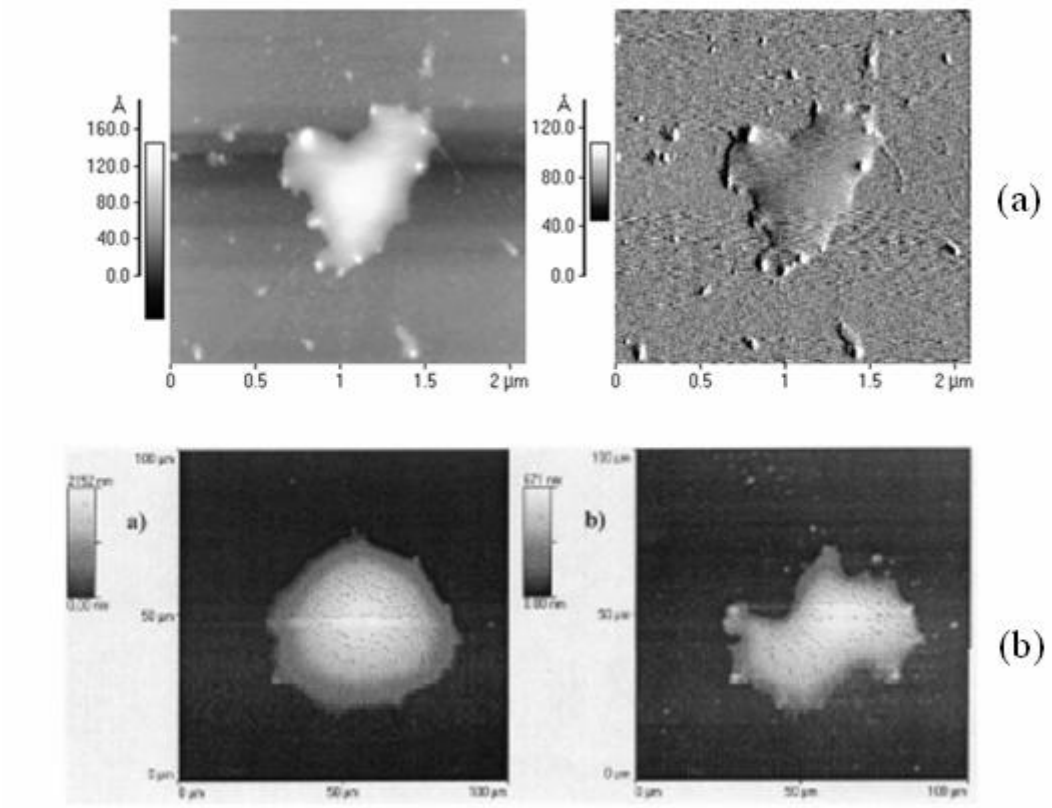

Fig. 5. (a) AFM images showing water micrometer-sized droplets-films, during the first stages of dewetting. (Left: topography; right: amplitude) [33]. (b) Dewetting sequence of a 1,5-pentanediol droplet right after deposition. The right image is taken 28 minutes after the left one. Note the similarity of both patterns (*a* and *b*-right), even at such different dimensional scales. Reproduced with permission from [34] © 2004 John Wiley & Sons.

Wettability at the mesoscopic level was evaluated by measuring the contact angle between nano-droplets and the silicon surface using AFM. The mean value of contact angle was (7.3±1.2)º. In this analysis, contact angles were measured at the very edge of the droplet profile. It is noticeable however, that many profiles presented a hat-like structure. Such a structure has been observed for a sub-microscopic droplet elsewhere [35,34]. Nanoscopic contact angles water/silicon wafer were compared by us with the values at macroscopic scale obtained by the sessile drop technique with a Drop Shape Analysis System. The mean nanoscopic contact angle (7.3º) was much lower than the measured macroscopic contact angle (27.8º). Results showed that the contact angle did not significantly change with the drop size in the studied range. The homogeneity of the surface in terms of hydrophilicity was confirmed within the chosen areas. It should be noted that recent researches have highlighted that nano-contact angles vary depending on the size of the nano-droplets [36,37,38] which depends on the environmental conditions and method used for creating them. At weak adhesion, the contact angle is found to grow steadily with the decrease of the drop size. This suggests a strong contribution of a positive line tension in the shape determination of the drop at equilibrium. At much stronger adhesion, however, the contact angle does not change with the drop size, and the line tension is approximately zero. In the studied range of drop sizes, no significant changes of the determined contact angle have been found due to the strong adhesion of water to silicon wafer surfaces.

Liu *et al.* [39] found by IC-AFM different structures on freshly cleaved mica treated with pure water. On the one hand, they observed water dots and islands. They interpreted the water pattern forming process as follows: the water meniscus forms when an AFM tip contacts the mica surface. It ruptures from the tip and dots appear. These structures can bear repeated scanning. They consider that a multilayer is formed and an ice-like structure exists inside these water structures. On the other hand they incubated several microliters of ultra-pure water for several minutes on freshly cleaved mica, then rinsed several times using pure water and dried with air. Some large network structures were imaged. The adjoined network segments were usually arranged close to 120º, consistent with epitaxy on the mica surface. The heights of the networks range from 2.1 to 3.3 nm, and the segment width from 40 to 100 nm. The authors concluded that these structures were not artefacts produced by the AFM tip or material transported from the AFM tip. As the network could be collapsed by the tip, Liu *et al.* speculated that the network was water or water bound to some unknown contaminant.

3.3. Scanning polarization force microscopy (SPFM)

Scanning polarization force microscopy (SPFM) [40], a SPM variant where a biased tip interacts with the liquid surface through long-range electrostatic forces, has been also successfully used to study water structures on solid surfaces at the nanoscale. This technique is based on the measurement of the polarization force between a charged AFM tip and the surface. Hu *et al.* [40] used this technique to analyze the structure of molecularly thin films of water on mica at different humid environments, controlled with a plastic box. They found different water structures on mica depending on the RH. When RH<20%, a uniform water layer, (5-10) nm in thickness (Phase I) was imaged. At RH>20-25 % they observed the formation of 2D domains (Phase II) that grew when the RH reached 40%. The apparent topographic height of these phase II regions is lower by 2 Å than the surrounding initial phase I. The polygonal shape of many boundary lines between phases I and II seems to indicate a crystalline structure for water in phase II. Hydrophobic mica was obtained after long exposure to air, possibly due to accumulation of contaminant material of organic origin. Any surface structure was imaged even at 99 %. However, water could be forced into the surface by contact with the tip at high humidity. A water droplet with an apparent height of 5 nm and diameter around 100 nm, by assuming a spherical shape, presented roughly a contact angle of 5º.

4. Comparing macroscopic and meso/nano-scopic wettability

Wang and coworkers [9,10] evaluated the wettability of water nano-droplets on mica (θ=10.8º), and metal surfaces (table 1) and related it to macro wettability results (31.4º , and table 1). They concluded that the nano-wettability was higher than the macro-wettability, but reasons for this were not found. When different surfaces were compared, lower macro contact angles corresponded to lower nano contact angles. They pointed out that the influence of organic contaminants on specimen surfaces might be one of the reasons. In general, organic contaminants give rise to a higher surface hydrophobicity, and their distribution may be not uniform [33] at the nano and/or meso-scale. In the case where droplets are obtained by condensation, as there should be places with less or no organic contaminants, water might be preferentially condensed on these places, resulting in the lower micro-wetting contact angles. In this line, results by Checco *et al.* [24] also point to the influence of small surface heterogeneities as the main responsible of the observed decrease in contact angle when their droplets decreased in size from 2 μm to 200 nm. The most wettable zones act as nucleation sites for the droplets, and this explains the lower contact angle of small droplets. If the droplet size becomes larger, then it extends beyond those more wettable nano- or meso-domains and the contact angles then increase. Their results shows that previous

interpretations of decreasing contact angle with decreasing size based solely on the line tension argument were irrelevant at microscopic scales [42].

Regarding the measurement of the liquid surface tension by AFM, Fraxedas *et al.* [19] predicted the surface tension of water nano-droplets in molecular nano-beakers and found a significantly larger value than the macroscopic one. They ascribed it to the nanometric length scale involved (collective modes of confined liquids). They speculated if water molecules might promote a hydrogen-bond network at the nano-droplet/air interface generating an ice-like structure, as Miranda *et al.* showed for water films on mica [43].

In relation to the derivation of the magnitude of the finite value of the line tension, the contact angle of a liquid droplet depends on its size [28]. In a large number of conventional contact angle goniometry experiments, variations of the contact angle with the radius of the droplet of the order of 1º have been reported for millimetre-sized droplets. These variations were interpreted in terms of a line tension of (10^{-5}-10^{-6}) N [14], which is four to six orders larger than predicted on theoretical grounds. Law and coworkers [44] obtained a value of 10^{-10} N using optical interferometry. Herminhaus and coworkers [27] obtained a CLT of liquid droplets on patterned surfaces of the order of 10^{-10} N using AFM. With homogeneous surfaces [28], they concluded that the strong drop size dependence of the contact angle, which is frequently observed in optical contact angle goniometry, is not caused by the line tension. Indeed, in the case of HEG droplets on silanized silicon substrates with radii between 1 and 3.5 mm, they found by optical measurements an average contact angle of 24º, and only an apparent increase in theta of 2º with decreasing radius. With AFM, and for droplets with radii between 380 and 8000 nm, an average value of 26º was obtained, and only a difference of 2º was found between the smaller and the bigger droplets. Based on the analysis of the profiles of the micro-sized droplet obtained by AFM near the three-phase contact line, the authors obtained an upper limit of 10^{-10} N for the line tension, whereas the sign could be either positive or negative, to the error associated to the measurement. For this system, important differences between macroscopic and submicroscopic contact angles are not observed. In addition, as discussed above, Checco *et al.* [24] concluded that observed AFM changes in the contact angle with the (microscopic) droplet size could not be fitted by the classical correction of τ. Trying to fit the correction on small portions of the experimental curves would not provide a fixed value for τ, but one that changed depending on the drop size.

Table 1: Compilation of meso/nano droplets geometrical characteristics. The contact angle of their macroscopic counterparts are also given.

Liquid and solid surface	Height (nm)	Radius (nm)	Meso/nano contact angle (º)	Macro-contact angle (º)	Ref.
Water on Pure Cr	6.7-21.1	25.6-42.9	44.2	76.8	[9]
Water on Mica	3.93-9.78	45.2-127	10.8	31.4	[9]
Water on wet polished Cr	6.7-37.8	25.6-74.1	40±10	80	[10]
Water on wet polished Ni	8.1-26	57.8-144.9	18±2	72	[10]
Water on wet polished Fe	12.6-35.6	72.5-248	17±4	68	[10]
Water on wet polished SUS304 steel	2.7-3.5	13.5-19.7	23±4	70	[10]
Water on oxidized Cr	4.2-22.9	22.8-162.5	20±5	70	[10]
Water on oxidized Ni	8.6-25.4	41.2-172.7	25±6	62	[10]
Water on oxidized SUS304 steel	6.6-53.9	217.2-317.5	7±2	70	[10]
Water on water immersed Cr	4.2-16.7	60.8-196.5	22±10	60	[10]
Water on water immersed Ni	13.9-40.7	110.5-202.8	16±4	68	[10]
Water on water immersed SUS304 steel	3-10.5	15.8-44.8	25±8	68	[10]
Water on SUS304 steel	5.2-32.4	39.6-111.2	22.5	68	[41]
Water on naturally oxidized Si	11 ± 5	215 ± 50	7.3	27.8	[32]
Water on magnetic recording disk	73	103	67.3	92	[29]
Water on mica	5	50	5	-	[40]
Ethanol on COOH terminated surface	-	-	12 ± 1	30 ± 1	[25]
Octane on OTS surface	-	-	9 ± 1	8 ± 1	[25]
Hydrocarbon oil on PS	5-12 nm	10-200	13 ± 2	14 ± 2	[6]
HEG on silanized silicon	-	380-8000	26	24	[28]

Acknowledgements The authors are grateful for financial support to: "Junta de Extremadura" (Regional Government) through project 3PR05A021, "Ministerio de Educación y Ciencia" (National Goverment) through the project MAT2006-12948-C04-03, FEDER, and "Fundación de Investigación Médica Mutua Madrileña".

References

[1] J. Lyklema, Fundamentals of Interface and Colloid Science, Vol. 1, Academic Press, 1993.
[2] A.W. Adamson, Physical Chemistry of Surfaces, 5th ed. John Wiley and Sons, NY, 1990.
[3] W. Duncan-Hewitt, Z. Policova, P. Cheng, E.I. Vargha-Butler and A.W. Neumann, Colloids and Surfaces **42**, 391 (1989).
[4] L. Sirghi, O. Kylin, D. Gilliland, G. Ceccone, and F. Rossi , Journal of Physical Chemistry B **110**, 25975 (2006)
[5] E. Bonaccurso, G. Gillies, Langmuir **20**, 11824 (2004).
[6] S.D.A. Connell, S. Allen, C.J. Roberts, J. Davies, M.C. Davies, S.J.B. Tendler and P.M. Williams, Langmuir, **18**, 1719 (2002).
[7] P.K. Hansma, V.B. Elings, C.E. Bracker and O. Marti, Science **242**, 209 (1988).
[8] G. Binnig, C. Gerber and C.F. Quate, Physical Review Letters **56**, 930 (1986).
[9] R. Wang, M. Takeda, M. Kido, Materials Letters **54**, 140 (2002).
[10] R. Wang, Li Cong, M. Kido, Applied Surface Science **191**, 74 (2002).
[11] A. Méndez-Vilas, M.G. Donoso, J.L. González-Carrasco and M.L. González-Martín, Colloids and Surfaces B: Biointerfaces **2**, 157 (2006).
[12] A. Méndez-Vilas, J.M. Bruque and M.L. González-Martín, Ultramicroscopy **107**, 617 (2007).
[13] G. Hong-Kai, F. Hai-Ping, Chinese Physics Letters **22**, 787 (2005).
[14] A. Amirfazli, A.W. Neumann, Advances in Colloid and Interface Science **110**, 121 (2004).
[15] T. Pompe, S. Herminghaus, Physical Review Letters, **85** (2000).
[16] J.F. Oliver, C. Huh, S.G. Mason, Journal of Colloid and Interface Science **59**, 568 (1977).
[17] R.J. Emerson and T.A. Camesano, Ultramicroscopy **106**, 413 (2006).
[18] W.F. Heinz and H.J. Hoh, Journal of Chemical Education **82**, 695 (2005), C.T. Gibson, D.A. Smith and C.J. Roberts, Nanotechnology 16, 234 (2005).
[19] J. Fraxedas, A. Verdaguer, F. Sanz, S. Baudron and P. Batail, Surface Science **588**, 41 (2005).
[20] T. Thorsen, S.J. Maerkl and S. R. Quake, Science, **298**, 580 (2002).
[21] D. Chatterjee, B. Hetayothin, A.R. Wheeler, D.J. King, R.L. Garrell, Lab Chip **6**, 199 (2006).
[22] H. Song, D.L. Chen and R.F. Ismagilov, Angew Chem Int Ed Engl. **45**, 7336 (2006).
[23] A. Gil, J. Colchero, M. Luna, J. Gómez-Herrero and A.M. Baró, Langmuir **16**, 5086 (2000).
[24] A. Checco, P. Guenoun and J. Daillant, Physical Review Letters **91**, 186101 (2003).
[25] A. Checco, Y. Cai, O. Gang and B. Ocko, Ultramicroscopy **106**, 703 (2006).
[26] V. Dupres, T. Camesano, D. Langevin, A. Checco and P. Guenoun, Journal of Colloid and Interface Science **269**, 329 (2004).
[27] T. Pompe, A. Fery and S. Herminghaus, Langmuir **14**, 2585 (1998).
[28] F. Mugele, T. Becker, R. Nikopoulos, M. Coñeen and S. Herminghaus, Journal of Adhesion Science and Technology **16**, 951 (2002)
[29] T.E. Karis and U.V. Nayak, Tribology Transactions **47**, 103 (2004).
[30] Karis, T. E. and Tawakkul, M. A., Tribology Transactions **46**, 469 (2003).
[31] C. Spagnoli, K. Loos, A. Ulman and M.K. Cowman, Journal of the American Chemical Society **125**, 7124 (2003).
[32] A.B. Jódar-Reyes, A. Méndez-Vilas, M.L.González-Martín, manuscript in preparation. Data available from authors.
[33] A. Méndez-Vilas, A.B. Jódar-Reyes, J. Díaz and M.L. González-Martín, submitted to Current Applied Physics (2007).
[34] S. Haferl, D. Poulikakos, and Z. Zhao, Experimental Heat Transfer 14, 1 (2001).
[35] W. Radigan, H. Ghiradella, H.L. Frisch, H. Schonhorn and T.K. Kwei, Journal of Colloid and Interface Science **49**, 241 (1974).
[36] G. Hong-Kai, F. Hai-Ping, Chinese Physics Letters **22**, 787 (2005).
[37] Y.T. Cheng, D.E. Rodak, A. Angelopoulos and T. Gacek, Applied Physics Letters **87**, 194112 (2005).
[38] I. Milchev and A.A. Milchev, Europhysics Letters **56**, 695 (2001).
[39] Z. Liu, Z. Li, H. Zhou, G. Wei,, Y. Song and L. Wang, Micron **36**, 525 (2005).
[40] J. Hu, X.D. Xiao, D.F. Ogletree and M. Salmeron, Surface Science **344**, 221 (1995).
[41] R. Wang, M. Kido, Materials Letters **57**, 2360 (2003).
[42] D. Quéré, Nature Materials **3**, 79 (2004).
[43] P.B. Miranda, L. Xu, Y.R. Shen and M. Salmeron, Physical Review Letters **81**, 5876 (1998).
[44] J. Y. Wang, S. Betelu and B.M. Law, Physical Review Letters **83**, 3677 (1999); J.Y. Wang, S. Betelu and B.M. Law, Physical Review Letters **E 63**, 031601 (2001).